Instruments and Experimental Techniques, Vol. 41, No. 5, 1998, pp. 701–705. Translated from Pribory i Tekhnika Eksperimenta, No. 5, 1998, pp. 118–122.

GENERAL
EXPERIMENTAL TECHNIQUES

Pyrolytic Graphite X-ray Echelon–Monochromator

A. G. Tur'yanskii and I. V. Pirshin

Lebedev Physical Institute, Russian Academy of Sciences, Leninskii pr. 53, Moscow, 117924 Russia

Received February 27, 1998

Abstract—A design of an X-ray echelon–monochromator based on semitransparent plates of pyrolytic graphite is described. The results of comparative tests of 0.5- to 1-mm-thick standard pyrographite monochromators, 46- to 180-μm-thick semitransparent plates, and an echelon–monochromator comprising three semitransparent plates are presented. An increase in the peak and integral reflectivity by 55 and 13%, respectively, is achieved in comparison to the best standard monochromator. The possibility of controlling the spectrum band is shown.

Pyrolytic graphite monochromators are widely used in X-ray measurements with radiation energies exceeding 5 keV. This is determined by the highest integral reflectivity R_s of pyrographite [1], the possibility of depositing pyrographite on surfaces of specified profiles [2, 3], and a simpler adjustment procedure due to a lower required angular adjustment accuracy than for Si, Ge, and quartz crystal–monochromators. However, the pyrographite peak reflectivity R_m, which is defined as the maximum ratio of the total intensity of diffracted radiation to the intensity of the incident quasi-parallel monochromatic beam, is smaller than the R_p of perfect Si crystals and multilayer X-ray mirrors [4, 5], for which $R_m > 0.7$. In addition, monolithic pyrographite plates and other crystal-based monochromators have fixed passbands that can be varied only by replacing the monochromator.

Here, we propose to replace a thick monolithic monochromator plate with a set of successive semitransparent plates, for which $(\mu_a + \mu_e)L < 1$, where μ_a is the linear attenuation coefficient, μ_e is the extinction coefficient, and L is the radiation path length in the material. As shown below, for mosaic pyrographite samples with mosaic blocks spread within an angle less than 0.6° in the diffraction position, the relation $\mu_e \geq \mu_a$ takes place. When the plates are separated along the beam by spacings, ensuring the free exit of the diffracted radiation, the effect of two negative factors—the attenuation caused by scattering and photoabsorption and the diffraction shielding by previous monochromator layers—simultaneously decreases. Therefore, when using an echelon of semitransparent plates, a significant increase in the reflectivity in comparison with a monolithic structure can be expected.

Pyrolytic graphite plates 0.5 and 1 mm thick (produced by the NII Grafite), supplied as monochromators for X-ray diffractometers, were taken as the initial material and reference samples.

Samples with an area of 0.6–0.9 cm^2 and thickness d = 46–180 μm were cut from these plates. The values of d presented in this paper were obtained by measurements of X-ray beam attenuation at fixed angles of incidence on the sample surface for the tabulated values of the density 2.23 g/cm^3 and mass attenuation coefficient 4.67 cm^2/g of pyrolytic graphite. Thickness measurements with a mechanical indicator yielded results that were overestimated by 10–20 μm for all plates. The most probable explanation for this effect is the roughness of their surfaces.

Figure 1 shows a diagram of the measuring system based on a ДРОН-3 diffractometer. The radiation from X-ray tube *1* with a copper anode was monochromated by Si(111) single crystal *2* rotatable about the axis O_1. The characteristic line Cu$K_{\alpha 1}$ was selected from the diffracted beam by a 0.05-μm-wide vertical slit *3*. The beam was additionally bounded and centered in the vertical plane by a 3-mm-wide horizontal slit *4*. The first *8* and third *10* pyrographite plates (along the X-ray beam propagation direction) were mounted on rotating sleeves *5* and *7* attached to heads for orienting single crystals. The heads provided translations of samples along the beam, perpendicular to it, and their rotations in the plane perpendicular to the beam. Plates *8* and *10* were independently adjusted for the angle of diffraction

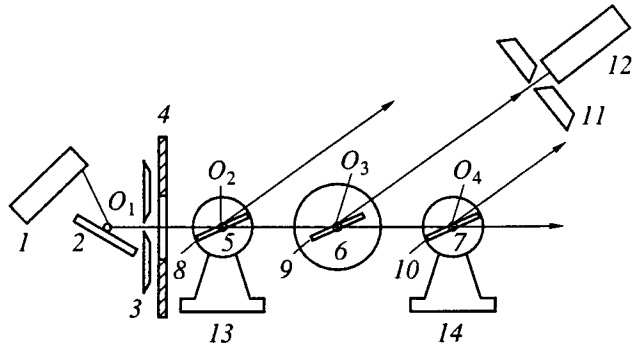

Fig. 1. Schematic diagram of the measuring system: (*1*) X-ray tube; (*2*) crystal–monochromator; (*3*, *11*) vertical slits; (*4*) horizontal slit; (*5*, *7*) rotating sleeves; (*6*) standard holder; (*8–10*) pyrographite plates; (*12*) detector; and (*13*, *14*) heads for single-crystal orientation.

0020-4412/98/4105-0701$20.00 © 1998 МАИК Наука/Interperiodica Publishing

by rotating the sleeves about axes O_2 and O_4 aligned with the X-ray beam plane during adjustment. The second plate *9* (along the beam propagation direction) was set in standard holder *6* for flat samples aligned with the principal axis O_3 of a horizontal type GUR-8 goniometer. The distance R between axis O_3 and the slit *11* was 190 mm, and the distances $s(O_2$–O_3 and O_3–$O_4)$ were 35 mm.

Before the plates were set in a row according to the diagram in Fig. 1, the following measurements of separate pyrographite samples were performed.

(1) Detector *12* was mounted on the incident-beam axis, and the radiation intensity I_0 was measured. Then, pyrographite plates were alternately placed into the central holder *6*. Plates were rotated and fixed at the angles $\Theta_1 = 15°$ and $\Theta_2 = 30°$, and the radiation intensities I_1 and I_2 transmitted through the sample were measured. The X-ray beam width near axis O_3 was below 100 μm. When our samples, with the width b = 6–8 mm, were set at an angle $\Theta > 10°$, their dimensions in the direction of the incident radiation were $b\sin\Theta >$ 1 mm, i.e., the samples obviously overlapped the incident beam. The plate thickness d was determined from the results of measuring the attenuation at the angles Θ_1 and Θ_2 (see table).

(2) In the detector position on the incident-beam axis, the angular position, in which the minimum transmitted beam intensity was observed (i.e., the diffraction-caused extinction was maximum), was found by rocking samples in the vicinity of the Bragg angle Θ_B. Angular dependences of the transmission intensity $I^T(\Theta)$ were recorded at a fixed detector position within an angular range of $\Theta_B - 2°$ to $\Theta_B + 2°$ (Fig. 2). Using this data, the angular half-width of the transmission curve $\Delta\omega_T$ (see table) and (by normalization) the angular dependence of the transmittance $T(\Theta)$ and T_{min} were found. The comparison of the relative intensity variation (Fig. 2) and T_{min} values shows that, as a result of extinction, the attenuation near the Bragg angle increases by a factor of approximately 2.

(3) Detector *12* was set to the maximum of the (0002) diffraction refection. At a fixed position of the detector with a 1-mm-wide receiving slit *11*, the reflected intensity $I^R(\Theta)$ was recorded within an angular range of $\Theta_B - 2°$ to $\Theta_B + 2°$. Then, the sample was removed, and a reference measurement of the incident-beam intensity I_0 was performed. The data allowed us to determine the integral reflectivity R_s, the peak reflectivity R_m, the half-width $\Delta\omega_R$, and (after normalization) angular dependences of the reflectivity $R(\Theta)$. These measurements were performed for the semitransparent plates and for the 0.5- and 1-mm-thick reference samples (see table). The minimum transmission and maximum reflection of the semitransparent plates were observed in the same angular positions.

The plates with the maximum ratio $R_m/(1 - T)$ were selected for placement in the echelon–monochromator. The echelon was adjusted with detector *12* set up on the forward-beam axis. Plates *8*–*10* were placed in holders *5*–*7*, respectively, and were adjusted sequentially. At first, each pyrographite plate was set parallel to the beam and was moved perpendicular to it until the maximum signal attenuation (caused by shutting the incident beam) was reached. Then, rotations about axes O_2–O_4 made it possible to find the angular position in which the minimum transmittance, corresponding to the maximum reflectivity, was provided (see above). Subsequently, angular scanning within a 2Θ range of $-2°$ to $+32°$ was performed with detector *12* (Fig. 3). The angular shift $2\Delta\Theta$ of diffraction peaks observed in the diagram is caused by the linear shift s in opposite directions of the axes of rotation of the first and third echelon plates, with respect to the detector axis of rotation. According to the measurement geometry in Fig. 1, the angular shift of the Bragg maximum is described by the following expression:

$$\Delta 2\Theta = \arctan\left(s\sin 2\Theta / \sqrt{R^2 - (s\sin 2\Theta)^2}\right). \quad (1)$$

Our setup has s = 35 mm and R = 190 mm, and we obtain $\Delta_1(2\Theta) = -\Delta_3(2\Theta) = 4.7°$, which is observed in

Characteristics of pyrographite monochromators

Sample	d, μm	$R_s \times 10^5$	R_m	T_{min}	$\Delta\omega_P$, degree	$\Delta\omega_T$, degree
Reference	1000	474	0.31	–	0.8	–
Reference	500	461	0.26	–	0.85	–
Reference	1000	527	0.28	–	1.05	–
Plate 1	76	290	0.29	0.46	0.56	0.56
Plate 2	46	204	0.22	0.60	0.50	0.50
Plate 3	71	300	0.28	0.47	0.57	0.56
Plate 4	180	370	0.25	0.26	0.82	0.92
Echelon (*P*)	193	541	0.47	0.13	0.61	–
Echelon (*N*)	193	595	0.35	0.23	0.92	–

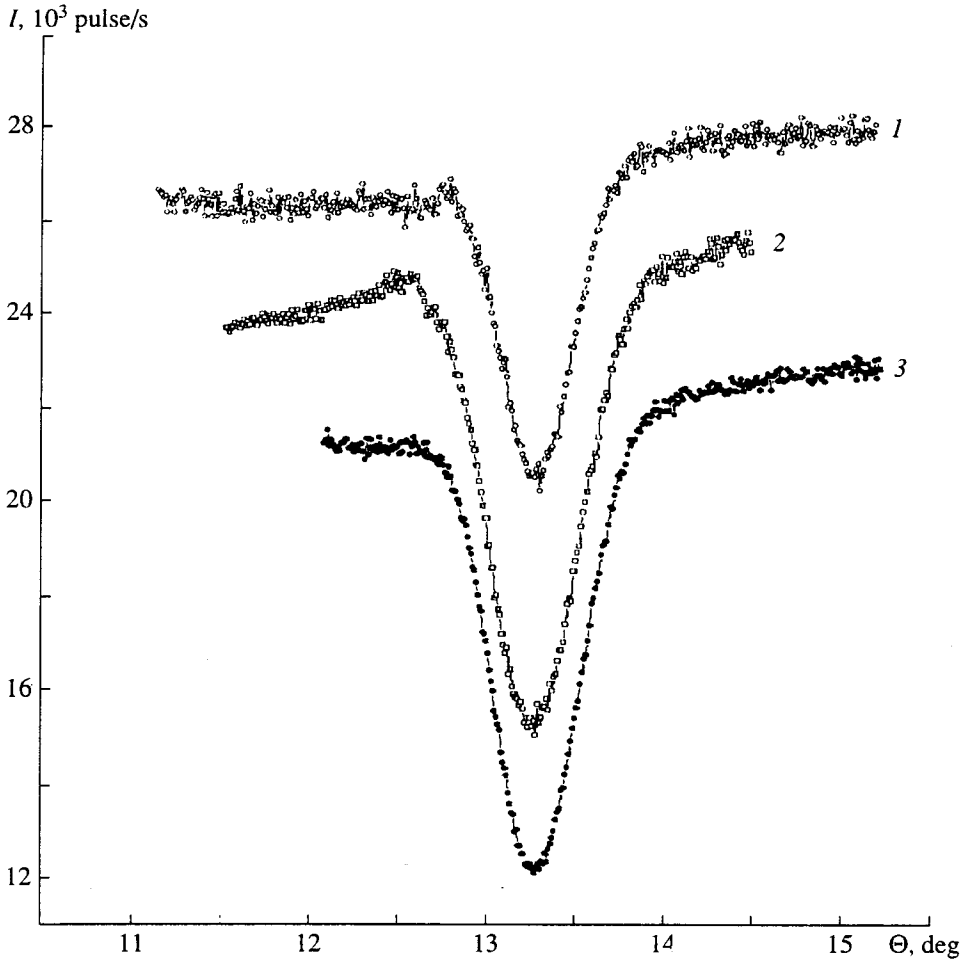

Fig. 2. Angular dependences of the transmission intensity under Θ-rocking (2Θ = 0 = const) for separate plates of the echelon–monochromator: (*1*) plates *8* (see Fig. 1); (*2*) plates *9*; and (*3*) plates *10*.

the angular diagram. The linear shift results in the same change in the angle of radiation incidence on the detector. However, since the angular variation is small, an increase in the attenuation in the beryllium window of the detector can be neglected.

When scanning was completed, a reference measurement of the incident-beam intensity I_0 was performed. The peak reflectivity R_m of the echelon was defined as $(I_{m1} + I_{m2} + I_{m3})/I_0$, where I_{m1}, I_{m2}, and I_{m3} are the intensity maxima in the angular diagram resulting from scanning. Because shafts O_2 and O_4 were not interconnected by an electromechanical drive, it was impossible to measure the integrated echelon reflection intensity for the synchronously rotating plates. According to measurements of angular profiles of incident and transmitted beams for samples with $d < 100$ μm, the angular profile broadening even in the diffraction position was about rocking 0.003°, i.e., negligibly small in comparison to the half-widths $\Delta\omega_R$ and $\Delta\omega_T$ of the curves for 2Θ = const (see table). This means that R_s and the angular dependences of the echelon reflectivity $R^e(\Theta)$ can be calculated from experimental reflection and transmission curves for each separate plate. In general, for an echelon consisting of n plates, we may write

$$R_s = \int_{\varphi_1}^{\varphi_2} R(\Theta)d\Theta = \int_{\varphi_1}^{\varphi_2} [R_1(\Theta + \Delta\varphi_i) + \sum_{i=2}^{n} R_i(\Theta + \Delta\varphi_i)\prod_{i=2}^{n} T_{i-1}(\Theta + \Delta\varphi_i)]d\Theta, \quad (2)$$

where $T_i(\Theta + \Delta\varphi_i)$ and $R_i(\Theta + \Delta\varphi_i)$ are the transmittance and reflectivity of the ith plate, respectively, $\Delta\varphi_i$ is the angle of deflection of the ith plate from the current angle Θ, and $[\varphi_1, \varphi_2]$ is the range of synchronized angular sweeping of the echelon plates ($\varphi_1 < \Theta_B < \varphi_2$). The angle of rotation of the first (entrance) echelon plate is convenient to be taken as the current angle. Then $\varphi_1 = 0$, and the other φ_i can be considered as angles of rotation of the echelon plates with respect to the entrance plate. As an example, Fig. 4 shows the measured dependence $R(\Theta)$ for the central echelon plate (curve *1*) and calcu-

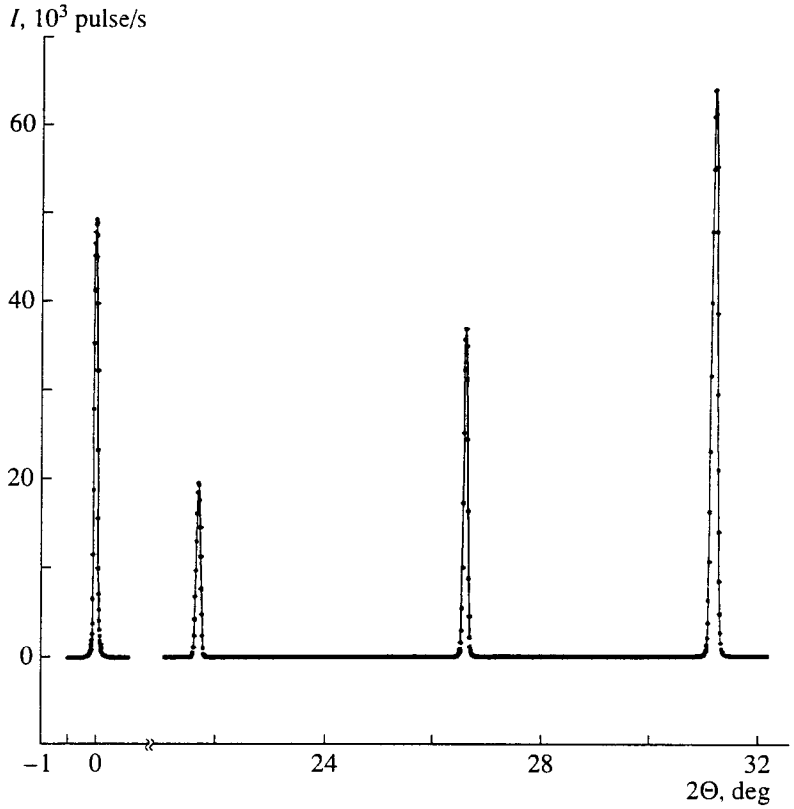

Fig. 3. Angular dependence of the reflection and transmission intensities of the echelon–monochromator for 2Θ-scanning with a detector (Θ = 13.2° = const).

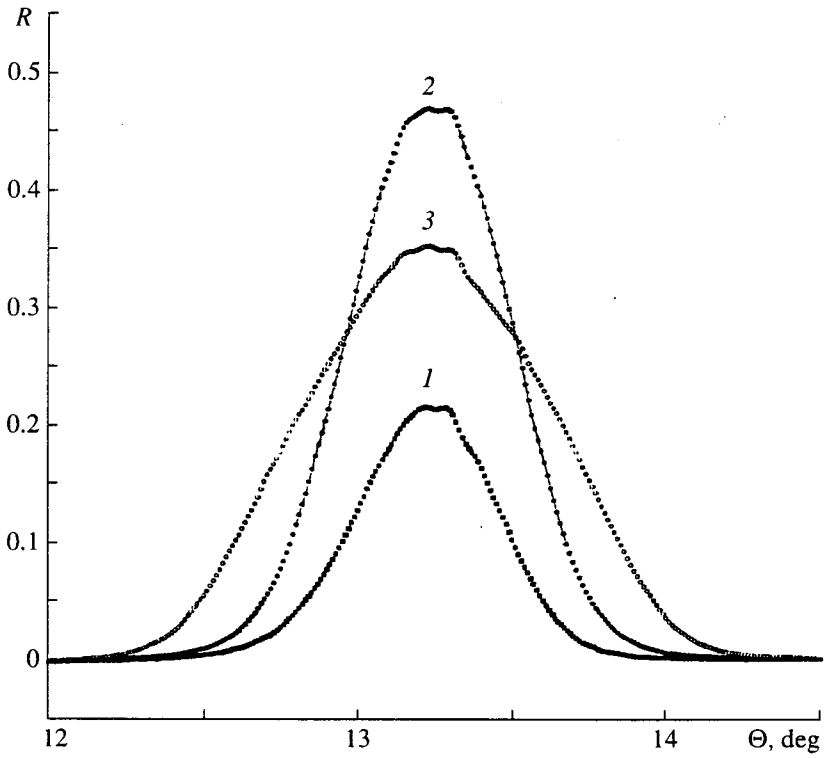

Fig. 4. Angular dependence of the reflectivity for Θ-rocking: (*1*) central plate of the echelon–monochromator; (*2*) echelon–monochromator with mutually parallel pyrographite plates; (*3*) echelon–monochromator with the second and third plates turned by 0.35° and –0.35°, respectively, relative to the first plate.

lated dependences for an echelon of three plates with zero angles of rotation (parallel orientation) and with the second and third plates turned by 0.35° and –0.35° with respect to the first plate (curves *2* and *3*). The echelon parameters corresponding to these orientations are labelled by the letters *P* and *N* in the table. As seen from the above data, nonzero angles of mutual plate rotation lead to a larger half-width of the function $R(\Theta)$ and, thus, to broadening of the passband of reflected and transmitted radiation. Note that, despite a decrease in R_m, R_s rises significantly, because the radiation attenuation due to extinction drops sharply. The same factor causes an almost twofold increase in the echelon transmittance in the nonparallel orientation.

The table shows that the optimally adjusted echelon–monochromator exceeds standard industrial specimens of massive pyrographite in the peak and integral reflectivities. However, in this case, monochromatic radiation is split into several beams. Note that the minimum acceptable distance O_2–O_3 and O_3–O_4 between the rotating echelon shafts equals the plate width (with the possibility of rotating past 360°). For the most widely used CuK_α radiation and $b = 6$ mm, the shift of the outer beams with respect to the central beam is 2.7 mm. The entrance window diameter of most of detectors exceeds 10 mm (e.g., 16 mm for БДС-7). Therefore, despite the beam splitting, the echelon-monochromated beam can be guided through a multiple-slit diaphragm to a single detector.

The proposed echelon–monochromator is especially efficient in X-ray reflectometers and small-angle cameras. It can also be utilized in X-ray diffractometers for phase analysis in the position of a crystal–analyzer. The potential of utilizing other properties of the echelon (selection of spectral lines and control of the operating spectrum band) will be considered in detail in the next paper.

REFERENCES

1. Freund, A.K., Munkholm, A., and Brennan, S., *Proc. SPIE-Int. Soc. Opt. Eng.*, 1996, vol. 2856, p. 69.
2. Antonov, A.A., Baryshev, V.B., Grigoryeva, I.G., *et al.*, *Nucl. Instrum. Methods Phys. Res., Sect. A*, 1991, vol. 308, p. 442.
3. Beckhoff, B., Kanngiesser, B., and Malzer, W., *Proc. SPIE-Int. Soc. Opt. Eng.*, 1996, vol. 2859, p. 190.
4. Vazina, A.A., Gerasimov, V.S., Kogan, M.T., *et al.*, *Apparatura i metody rentgenovskogo analiza* (Equipment and Methods for X-ray Analysis), 1981, no. 26, p. 3.
5. Barbi, T.Jr., *X-ray Microscopy*, Schmahl, G. and Rudolf, D., Eds., Geidelberg: Springer, 1984. Translated under the title *Rentgenovskaya optika i mikroskopiya*, Moscow: Mir, 1987, p. 204.